Evolution of a shocked multimode interface with sharp corners

Xu Guo, Juchun Ding, Xisheng Luo, and Zhigang Zhai*
Department of Modern Mechanics, University of Science and Technology of China, Hefei 230026, China

(Received 19 May 2018; published 26 November 2018)

Richtmyer-Meshkov instability of an inverse-chevron air/SF_6 interface subjected to a weak shock wave is experimentally studied. The inverse-chevron interface is a typical configuration that possesses multimode features and sharp corners. Using the soap film technique, five inverse-chevron interfaces with different initial vertex angles are generated to highlight the effects of initial amplitude-wavelength ratio on flow characteristics. A high-speed Schlieren system is used to observe the postshock flow field. After shock impact, a vortex pair is derived from the upstream interface, and the scale of the vortex pair is sensitive to the initial amplitude-wavelength ratio. The width growth in the linear phase is measured and compared with the classical impulsive model and a modified model considering a velocity reduction factor, and the latter is proven to be effective for moderate to large initial amplitudes. The linear growth rate is also a nonmonotone function of the amplitude-wavelength ratio. Further comparison with our previous work illustrates that the amplitude-wavelength ratio corresponding to the maximum width growth rate is associated with the Atwood number, which is consistent with the previous numerical results. A weakly nonlinear growth is observed at late stages, which deviates from the predictions of most typical nonlinear models. Finally, an empirical model is proposed that provides a satisfactory prediction of width growth in linear and weakly nonlinear stages.

DOI: 10.1103/PhysRevFluids.3.114004

I. INTRODUCTION

Richtmyer-Meshkov (RM) instability [1,2] occurs when an initially perturbed interface separating two fluids with different densities is impulsively accelerated, such as by shock waves. The perturbation amplitude will grow with time, and the growth generally experiences a linear phase, and then a nonlinear phase, and eventually a turbulent mixing state. The RM instability plays an important role in many areas of scientific research, such as inertial confinement fusion (ICF) [3] and astrophysical problems [4]. In the past few decades, much attention has been paid to RM instability, and several comprehensive reviews have been presented [5–9].

During the development of single-mode interfaces after shock impact, the formation of spikes (a heavier fluid penetrating into a lighter fluid) and bubbles (a lighter fluid penetrating into a heavier fluid) indicates the nonlinear growth of perturbation. To figure out the differences in growth rates between spikes and bubbles, the evolution of a single-mode interface with different initial wavelengths was studied by Sadot *et al.* [10]. In their experiments, the growth rate of spikes was larger than that of bubbles, and the disparity was aggravated in the nonlinear stage. Jacobs and Krivets [11] also experimentally studied the perturbation development of a single-mode interface, and similarly the spikes developed faster than the bubbles. Numerically, the discrepancies in width growth rates between spikes and bubbles of a single-mode interface were investigated by Dimonte and Ramaprabhu [12], and they obtained similar conclusions to those of Sadot *et al.* [10] and Jacobs

*sanjing@ustc.edu.cn

and Krivets [11]. Consequently, for single-mode interfaces, the spikes behave differently compared with the bubbles. The previous work showed that the spike is more unstable than the bubble, and the width prediction of the spike is more difficult than the bubble [13–15].

In most practical applications, however, the material interface is generally multimode, and often has sharp corners. For example, the surface of the ICF target may not be absolutely smooth, but it has sharp corners, and the perturbations are essentially random. It is, therefore, necessary to investigate the evolution of a multimode interface with sharp corners. A chevron or an inverse-chevron interface is a fundamental and typical configuration that possesses multimode features and sharp corners [16]. An inclined interface (half-chevron interface) was often encountered in shock refraction problems [17–19], but little attention has been placed on the interface evolution. An interface with sawtooth initial perturbations was created by the nitrocellulose membranes to highlight the high-amplitude effects [20]. Recently, McFarland *et al.* [21–24] carried out a series of studies on the RM instability of an inclined interface by numerical, experimental, and theoretical methods, and fruitful achievements were made. Numerical simulations on the inclined interface have also been performed by Samtaney and Zabusky [25] to study the vorticity production and vortex dynamics because the angle of an inclined interface is constant, which provides a controllable parameter for analyzing the baroclinic vorticity generation. As pointed out by Zhang *et al.* [26], a chevron or an inverse-chevron interface is also a fundamental geometry used in studying accelerated inhomogeneous flows. In our previous work [27,28], a soap film technique was adopted to create a chevron interface, and the width growth was obtained. The conclusion that the linear growth rate of the width is a nonmonotonic function of the initial amplitude-wavelength ratio, drawn by Dell *et al.* [29] for single-mode interfaces, was verified by our experiments. The nonlinear model proposed by Dimonte and Ramaprabhu [12] was found to be applicable for predicting the width growth of a chevron interface. A chevron interface can be approximately regarded as a spike configuration, while an inverse-chevron interface can be approximately regarded as a bubble configuration. Due to the existence of a sharp corner and multimode features, the differences in width growth between chevron and inverse-chevron interfaces needs special consideration, and it should be examined whether the existing models proposed for single-mode interfaces can predict the width growth of the inverse-chevron interface.

In this work, the RM instability of an inverse-chevron interface is investigated experimentally. Five inverse-chevron interfaces with different amplitude-wavelength ratios are generated using the soap film technique, and the postshock flow field is captured by Schlieren photography combined with a high-speed video camera. Some models will be considered to estimate the width growths in linear and nonlinear stages. Finally, we will attempt to bridge the initial and asymptotic velocities of width growth by proposing a nonlinear empirical model.

II. EXPERIMENTAL METHODS

The soap film technique has already proven its feasibility and reliability to generate a chevron interface [27] and a polygonal interface [30]. Thus, only a brief description of this technique is given here. As shown in Fig. 1(a), the interface framework with a depth of 20 mm is first manufactured by two Acrylic sheets (3 mm in thickness) for interface formation. To avoid pressure singularity, thin wires (0.128 mm in diameter) will be introduced at interface vertexes, and the number of thin wire is dependent upon the vertex angle. As indicated in previous work [27,31], at least three wires are needed for the vertex angle $\theta \leqslant 60^\circ$ and only one wire is needed for $\theta \geqslant 120^\circ$. In this work, as sketched in Fig. 1(b), when $\theta = 60^\circ$, three wires are arranged at points A, B, and C, respectively, to guarantee the angle $\alpha \geqslant 120^\circ$. In other words, the interface vertex point is shifted from D to B. To minimize the effects of initial interface deformation, the length of BD is requested to be as small as possible. However, the soap film interface is difficult to generate if the length of AB is shorter than 1 mm. In this work, provided that the angle $\alpha \geqslant 120^\circ$, the lengths of AB and BD are chosen as 1.24 and 1.55 mm, respectively, and the value of angle α is determined to be 137°. Similarly, when $\theta = 90^\circ$, the lengths of AB and BD are chosen as 1.11 and 0.7 mm, respectively, and the angle α is

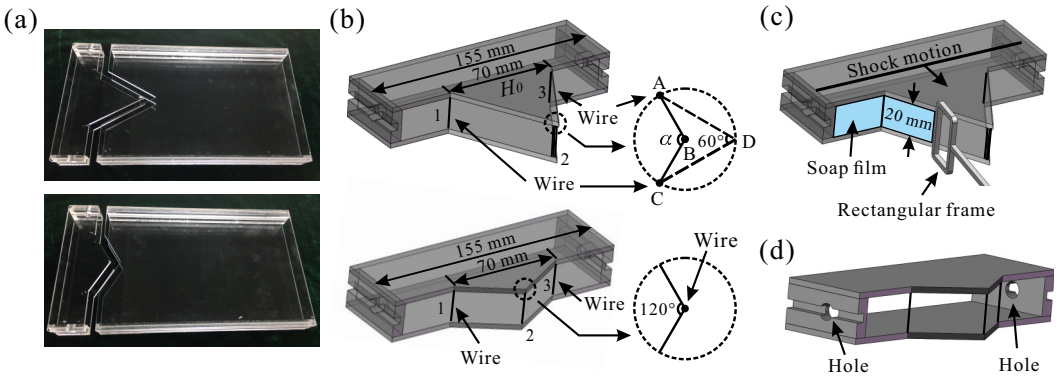

FIG. 1. The interface formation method. The Acrylic model used in experiments (a), arrangement of wires at the vertex for $\theta = 60^\circ$ and 120° (b), interface formation device (c), and the holes on the framework walls (d).

143°. Before generating the interface, the framework edges are wetted by a mixed solution (made of 60% clean water, 20% concentrated soap liquid, and 20% glycerin by volume) prepared in advance. Then, as shown in Fig. 1(c), by pulling a rectangular frame along the edges of the framework, an inverse-chevron soap film interface can be generated. Two holes are opened symmetrically on the framework walls, as shown in Fig. 1(d), to guarantee the pressure balance inside and outside the shock tube. Note that two flat interfaces are added between the inverse-chevron interface and the tube wall to reduce the wall effects on interface evolution. As a result, the interface is not a periodic inverse-chevron one, which has some differences of wave patterns near the wall compared with a periodic one. From our previous work [27,32], the influence of boundary-layer thickness on interface evolution can be neglected. Also the three-dimensional effect of the initial interface is limited. In this work, five inverse-chevron interfaces with different initial vertex angles ($\theta = 60^\circ$, 90°, 120°, 140°, and 160°) are generated, and the initial interface height H_0 is fixed to be 70 mm for all cases. Similar to our previous work [27], the wavelength (λ) is defined as $2H_0$, and the initial amplitude (a_0) is taken to be the width of the entire initial interface. Then the relationship among λ, a_0, and θ can be given as $a_0/\lambda = (1/4)\cot(\theta/2)$.

When the soap film interface is formed, the interface framework is inserted into the test section. To generate an air/SF_6 interface, air at the right side of the interface must be exhausted and replaced by SF_6. For this purpose, SF_6 is injected from the end of the test section, and air is discharged through another hole in the test section. An oxygen concentration detector is placed near the hole to monitor SF_6 purity in the test section. In our experiments, when the volume fraction of oxygen is reduced to 6%, the inflation process is stopped. Note that an appropriate inflation rate is needed to protect the formed interface. After the air/SF_6 interface formation and prior to the experiment, the time interval allows the diffusion between gases through the interface. In this work, the gas concentrations at both sides of the interface are determined by the velocities of incident and transmitted shock waves measured from the Schlieren images and one-dimensional (1D) gas dynamics theory. The actual gas concentrations are listed in Table I. The gas contamination at the left side of the interface will result in a slight increase of the incident shock Mach number with about 0.01. Also the Atwood number, defined as $A = (\rho_2 - \rho_1)/(\rho_2 + \rho_1)$, with ρ_2 and ρ_1 being the densities of gases at the right and left sides of the interface, respectively, will be affected by gas contamination.

The experiments are conducted in a horizontal shock tube, which consists of a 1.7-m-long driver section, a 3.9-m-long driven section, and a 1.0-m-long test section with a 155×26 mm^2 cross-sectional area. The Mach number of the incident shock wave propagating in pure air is Ma $= 1.22 \pm 0.01$, which indicates that the shock tube facility has a very good repeatability. Illuminated by a dc regulated light source (DCR III, SCHOTT North America, Inc.), the postshock flow is captured

TABLE I. Experimental parameters for five cases. Ma is the Mach number of an incident shock wave, VFL (VFR) is the volume fraction of SF_6 at the left (right) side of the interface, A^+ is the postshock Atwood number, and Δv is the jump velocity for a flat interface calculated by 1D gas dynamics.

Case (θ)	60	90	120	140	160
a_0/λ	0.433	0.250	0.144	0.091	0.044
Ma	1.235	1.236	1.235	1.238	1.229
VFL (%)	6.6	6.7	6.2	7.6	3.9
VFR (%)	59.5	58.5	57.5	61.5	59.5
A^+	0.488	0.480	0.482	0.484	0.524
Δv (m/s)	87.06	87.50	87.72	86.63	86.89

by Schlieren photography combined with a high-speed video camera (FASTCAM SA5, Photron Limited). The frame rate of the high-speed video camera is 50 000 fps with an exposure time of 0.368 μs, and the pixel resolution is about 0.32 mm pixel^{-1}.

III. RESULTS AND DISCUSSION

A. Interface morphology and features

The experimental Schlieren frames of a shocked inverse-chevron interface with different initial vertex angles are shown in Fig. 2. The initial time is defined as the moment when the incident shock wave (IS) contacts the interface. As indicated in Fig. 2(a), as the IS propagates along the interface, the refraction shock wave (RS) and the reflected shock wave (RFS) are generated. When the IS completely passes through the interface, the RFS is also transmitted through the interface, forming the reflected-transmitted shock wave (RTS) [Fig. 2(a) at $t = 186\,\mu$s]. A prominent vortex pair is derived from the corner of the upstream interface due to baroclinic vorticity deposition, and many small vortices are gradually generated on oblique interfaces that may be ascribed to RM instability and Kelvin-Helmholtz shear instability. The original sharp corner of the downstream interface becomes blunt, and its scale gradually increases in the spanwise direction due to the induction of vorticity deposited on oblique interfaces [Fig. 2(a) at $t = 546\,\mu$s]. As time passes, the scale of the upstream vortex pair increases slowly with the surrounding fluids gradually being entrained into the vortical structure [Fig. 2(a) at $t = 546$–$1566\,\mu$s]. As θ increases, the upstream vortex pair becomes obscure because of less vorticity deposition. At late stages, a stratified interface can be observed, as indicated by dashed rectangles in the Schlieren frames for $\theta = 90^\circ$. Note that small gaps between the Acrylic sheet and the optical glass will exist because they are not fixed very tightly. A small amount of SF_6 gas will diffuse into this space, and the Schlieren image in the test section is superimposed by another interface of air/SF_6 between the Acrylic sheet and the optical glass. Fortunately, the interface in the test section we are concerned with will not be influenced by the interface located at the space between the Acrylic sheet and the optical glass because they are located at different spaces separated by the Acrylic sheet.

Time variation of upstream vortex spacing (Lw), defined in Fig. 2, is given in Fig. 3 with error bars representing the measurement uncertainty in experiments. The vortex spacing for $\theta = 160^\circ$ is omitted because the vortex pair is not fully developed so that the vortex core cannot be clearly identified. The vortex spacing decreases as time elapses for all cases, because the interface velocities induced by vorticity deposited on the upper (lower) inclined interface have a component in the vertical direction, making two primary vortices moving toward the central axis gradually. As θ increases, less vorticity is generated, and the upstream vortex spacing becomes larger. A nonlinear variation of the vortex spacing is found for all cases because the upstream vortex pair gradually engulfs smaller vortices on oblique interfaces, which will affect the position of the vortex core. Moreover, the displacement of the downstream interface in the streamwise direction (Ls), defined as the distance to the initial interface vertex, and the width of the downstream interface in the spanwise

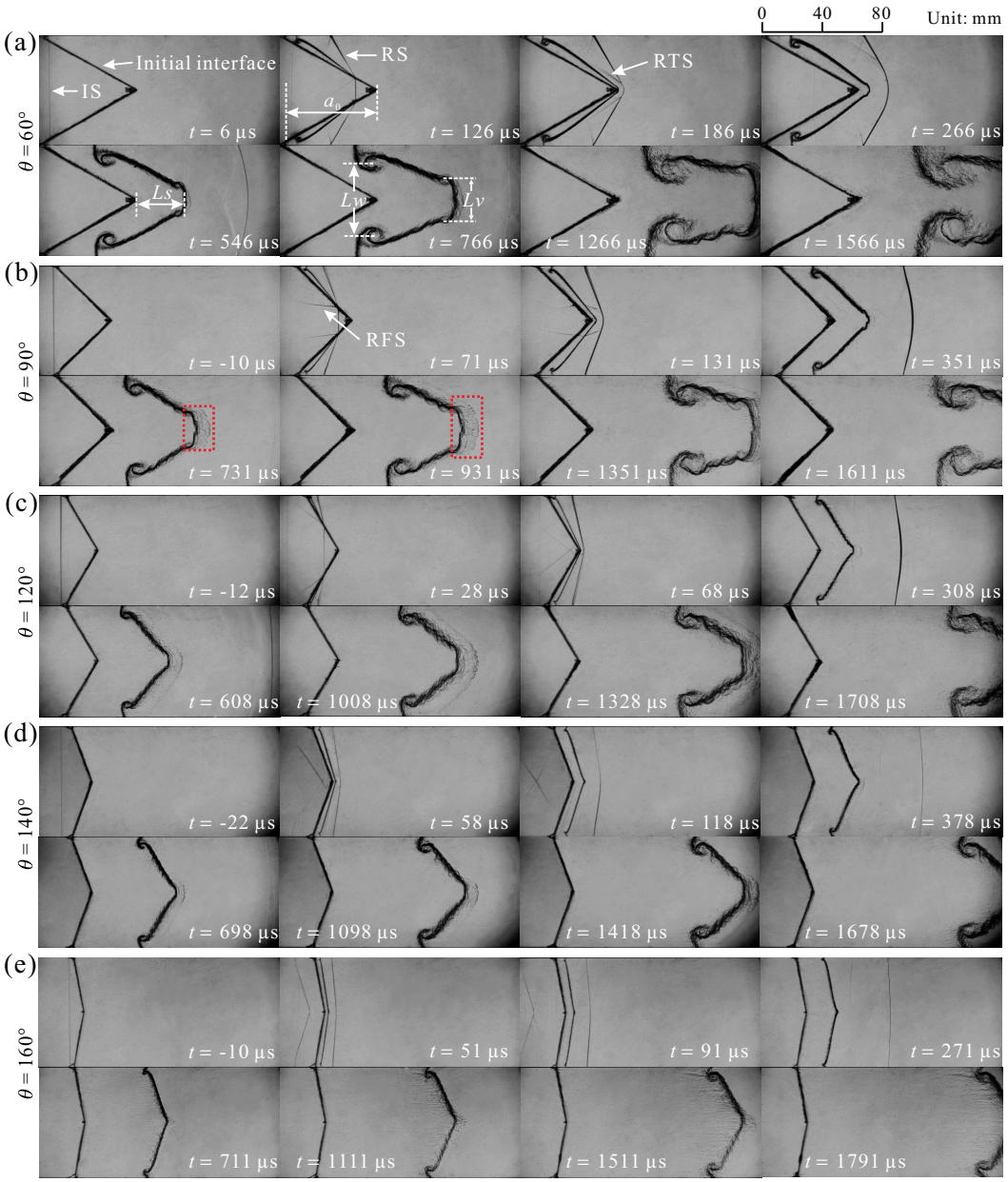

FIG. 2. Experimental Schlieren images of an inverse-chevron air/SF_6 interface impacted by a planar shock wave for $\theta = 60^\circ$ (a), $\theta = 90^\circ$ (b), $\theta = 120^\circ$ (c), $\theta = 140^\circ$ (d), and $\theta = 160^\circ$ (e). IS denotes the incident shock wave, RS denotes the refracted shock wave, a_0 is the initial interface amplitude, RFS is the reflected shock wave from the interface, RTS is the refracted shock wave of the RFS through the interface, Ls is the displacement of the downstream interface, Lw is the upstream vortex spacing, and Lv is the separation displacement of two inclined interfaces.

direction (Lv) at early stages are presented in Fig. 4. The spanwise scale of the downstream interface for $\theta = 160^\circ$ is ignored for its very small deformation. Nearly linear movements of the downstream interface in both the streamwise and spanwise directions are found for each case, and the velocities (v_h in the streamwise direction and v_p in the spanwise direction) obtained by linear fitting of the

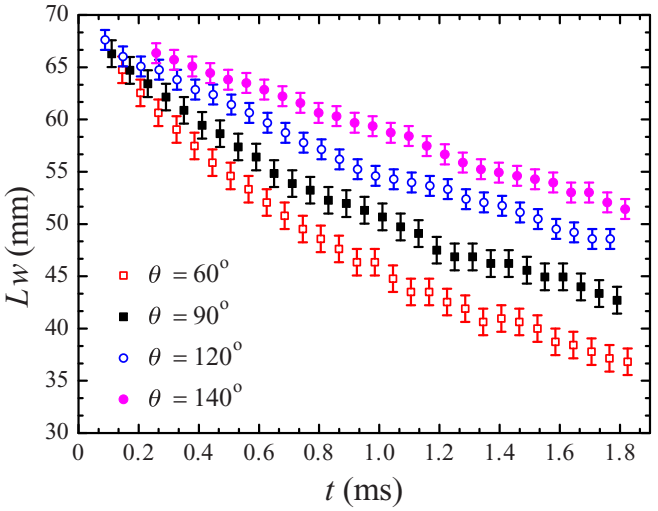

FIG. 3. Time variation of the vortex spacing for four cases ($\theta = 60^\circ$, 90°, 120°, and 140°).

experimental points are also presented in Fig. 4. As θ decreases, generally the downstream interface moves faster and the spanwise scale varies greatly because of the induction by more vorticity deposited on the interface.

B. Linear stage of interface width growth

After the incident shock passes through the perturbed interface completely, the interface width begins to grow, and a bubble structure appears. For a sinusoidal interface with a small initial amplitude, a classical impulsive model [1] was proposed to predict the width growth, which can be expressed as

$$a = a_0^+ + a_0^+ \Delta v k A^+ t, \tag{1}$$

where a_0^+, k, and A^+ are the postshock amplitude, the wave number ($k = 2\pi/\lambda$), and the postshock Atwood number, respectively. However, the impulsive model is only valid when the initial amplitude is small enough ($a_0/\lambda < 0.1$), as indicated by dashed lines in Fig. 5. A modified model including

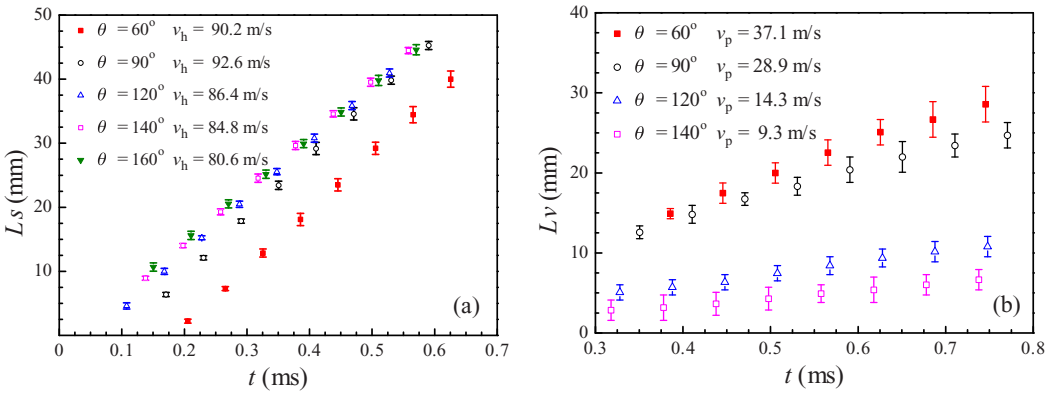

FIG. 4. Time variations of the downstream interface displacement in the streamwise direction (Ls) (a), and of the width of the downstream interface in the spanwise direction (Lv) (b) at early stages.

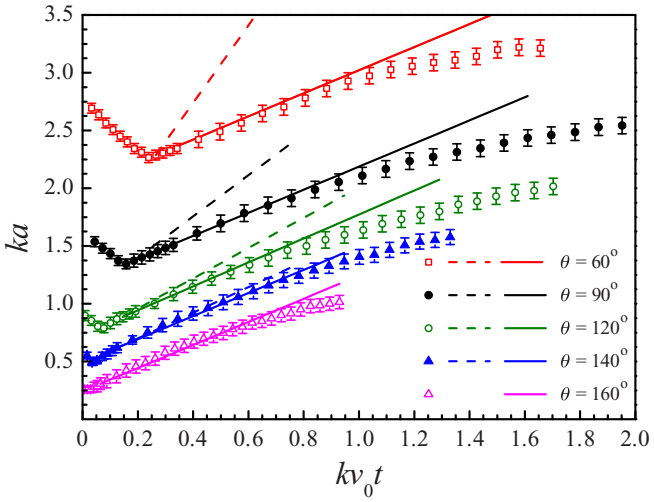

FIG. 5. Comparison of interface width growth in a linear stage between experiments and theoretical predictions. Symbols: experiments; dashed lines: the impulsive model [1]; solid lines: the modified model [20].

a velocity reduction factor R was proposed by Rikanati *et al.* [20], which can be applied to both sinusoidal and chevron interfaces with high initial amplitudes. The model can be described as

$$a = a_0^+ + a_0^+ \Delta v k A^+ t * R, \tag{2}$$

where

$$R = u_0(a)/u_0^{\mathrm{lin}}(a),$$

$$u_0(a) = -\mathrm{Re}\left[f \int_0^{\lambda} \frac{\sin[\phi^-]}{\cos[\phi^+]} \times \cot\{\pi/2[-x + i a_0 f_p (1 - y(x))]/\lambda\}\, dx \right],$$

$$u_0^{\mathrm{lin}}(a) = -a\,\mathrm{Re}\left[-f \int_0^{\lambda} \pi \sin(\pi x/\lambda) \cot(-\pi/2x\lambda)\, dx \right].$$

In these equations, u_0 is the initial tip velocity induced by a general periodic vorticity distribution on an interface [33], and u_0^{lin} is the tip velocity obtained from the impulsive model. $\phi^{\mp} = \arctan(dy^{\mp}(x)/dx)$, where ϕ^- is the local preshock inclination angle between the interface and the incident shock wave, and ϕ^+ is the postshock inclination angle. $y(x)$ is the shape function of the initial interface, and f is a function related to vorticity per unit length deposited on a straight interface by an oblique shock wave [25]. For angles smaller than the Mach reflection critical angle, deposited vorticity per unit length can be given by

$$\frac{d\Gamma}{ds} = f(M, \rho_1, \rho_2, \gamma_1, \gamma_2, p_1, p_2) \sin\phi + O(\sin^3\phi).$$

The velocity reduction factor R is crucial to correct the width growth rate of the interface with high initial amplitudes. The values of R calculated based on the expression above for five cases are listed in Table II. Through time derivation of interface width a, the linear growth rate v_0 can be given by

$$v_0 = \frac{da}{dt} = a_0^+ \Delta v k A^+ * R. \tag{3}$$

TABLE II. The velocity reduction factor R, the postshock amplitude a_0^+ with errors smaller than 1 mm, and the linear growth rate v_0 from experiments for five cases.

Case (θ)	60	90	120	140	160
R	0.299	0.560	0.791	0.905	0.976
a_0^+ (mm)	50.48	30.04	17.62	11.32	5.89
v_0 (m/s)	26.50	30.78	25.09	21.30	14.74

According to Eq. (3), time variation of the interface width growth in normalized form is presented by solid lines in Fig. 5, and the values of postshock amplitude a_0^+ are listed in Table II. Compared with the impulsive model, the revised model considering a reduction factor gives a reasonable prediction for the width growth in the linear phase.

In our previous work [27,28], the linear growth rate of a chevron interface is a nonmonotone function of θ, which experimentally verifies the numerical results obtained by Dell *et al.* [29]. In this work, similarly, the linear growth rates v_0 for five cases are obtained from experiments, and the values are listed in Table II. The experimental results also show a nonmonotone function of v_0 with θ. Theoretically, the linear growth rate is given by

$$\bar{v} = \frac{2v_0 a_0}{\pi A^+ a_0^+ \Delta v} = R\cot(\theta/2), \tag{4}$$

where $\bar{v}$ is only a function of θ, and the relationship between $\bar{v}$ and θ is obtained as indicated in Fig. 6. A nonmonotone relation between $\bar{v}$ and θ is observed, and the theoretical results agree well with the experimental counterparts. The maximum v_0 is obtained at $a_0/\lambda = 0.284$, i.e., $\theta = 82.8^\circ$, which is different from our previous work where the maximum v_0 was obtained at $a_0/\lambda = 0.25$, i.e., $\theta = 90^\circ$. Nevertheless, the value of a_0/λ at which the maximum v_0 is obtained is still located within the range 0.2–0.4 proposed by Dell *et al.* [29]. Dell *et al.* [29] once pointed out that the value of a_0/λ when the maximum v_0 is reached is slightly dependent on the shock Mach number and the Atwood number. Compared with our previous work [27], the shock Mach number in this work is nearly the same while the preshock Atwood number is smaller. Therefore, we can claim that the experimental data are consistent with the statement that the value of a_0/λ corresponding to the maximum v_0 is associated with the Atwood number.

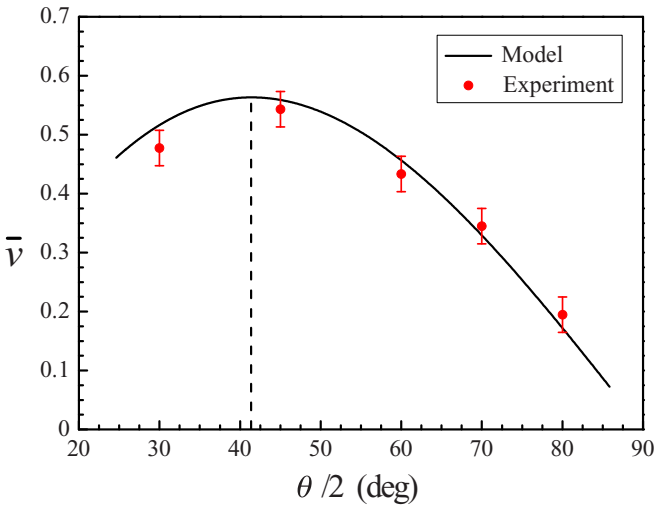

FIG. 6. Variation of the width growth rate with initial amplitude from experiments and model.

C. Nonlinear stage of interface width growth

In the late stage of interface evolution, an obviously nonlinear feature is observed. For single-mode interfaces, some empirical nonlinear models have been developed to bridge the initial and asymptotic phases. Here these models are checked for the inverse-chevron interface.

Sadot *et al.* [10] proposed a nonlinear model (the SEA model) to capture the linear and nonlinear growths of bubbles and spikes. This model can be described as

$$v_{b/s}^{\mathrm{SEA}} = v_0 \frac{1+\tau}{1+(1\pm A^+)\tau + [(1\pm A^+)/(1+A^+)][1/(2\pi C)]\tau^2}, \tag{5}$$

where $\tau = kv_0 t$, and $C = 1/(3\pi)$ for $A^+ \gtrsim 0.5$ and $1/(2\pi)$ for $A^+ \to 0$. In this model, a term $1 \pm A^+ \propto \tau$ is adopted in the denominator for bubbles and spikes, which is simple and is not related to ka_0^+. The quadratic term in the denominator is required to obtain asymptotic velocities, which takes different values for large or small A^+. It should be mentioned that the linear and quadratic terms in the denominator both take "+" for bubbles and "−" for spikes, which makes the asymptotic growth of bubbles enter the saturation phase faster than that of spikes. The SEA model was verified to be successful for predicting the width growth of an air/SF_6 single-mode interface [34], an air/CO_2, or an air/SF_6 single-mode interface with high amplitudes [35]. In this work, the SEA model can also provide satisfactory predictions for the width growth, as illustrated in Figs. 7(a)–7(e), when the constant C is $1/(2\pi)$ rather than $1/(3\pi)$.

For a single-mode interface, based on analytical solutions to potential flow equations, Mikaelian [36] proposed a nonlinear model (the MIK model) to bridge the initial and asymptotic stages of bubble growth that was given by

$$v_b^{\mathrm{MIK}} = v_0 \frac{1}{1+[3(1+A^+)/(3+A^+)]\tau}. \tag{6}$$

In this model, the asymptotic velocity agrees with the results of Oron *et al.* [37] and Goncharov [38]. In the work of Jacobs and Krivets [11], the MIK model succeeded in capturing the bubble growth rates for two single-mode interfaces with different wavelengths. Unfortunately, the MIK model cannot capture the nonlinear growth of the inverse-chevron interface in this work, as shown in Fig. 7. This may be due to the fact that the model was derived based on a single-mode interface, and it lacks a suitable quadratic term to better obtain the asymptotic velocity.

According to the evolution of a single-mode interface, Dimonte and Ramaprabhu [12] proposed a nonlinear model (the DR model) through numerical simulations, which can be expressed as

$$v_{b/s}^{\mathrm{DR}} = v_0 \frac{1+(1\mp|A^+|)\tau}{1+C_{b/s}\tau + (1\mp|A^+|)F_{b/s}\tau^2}, \tag{7}$$

where

$$C_{b/s} = \frac{4.5 \pm |A^+| + (2\mp|A^+|)|ka_0^+|}{4}, \quad F_{b/s} = 1 \pm |A^+|.$$

The DR model is similar to the SEA model in form. In the numerator, a term $1 \mp |A^+| \propto \tau$ is used to describe an acceleration of bubbles and spikes, respectively. In the denominator, a coefficient $C_{b/s}$

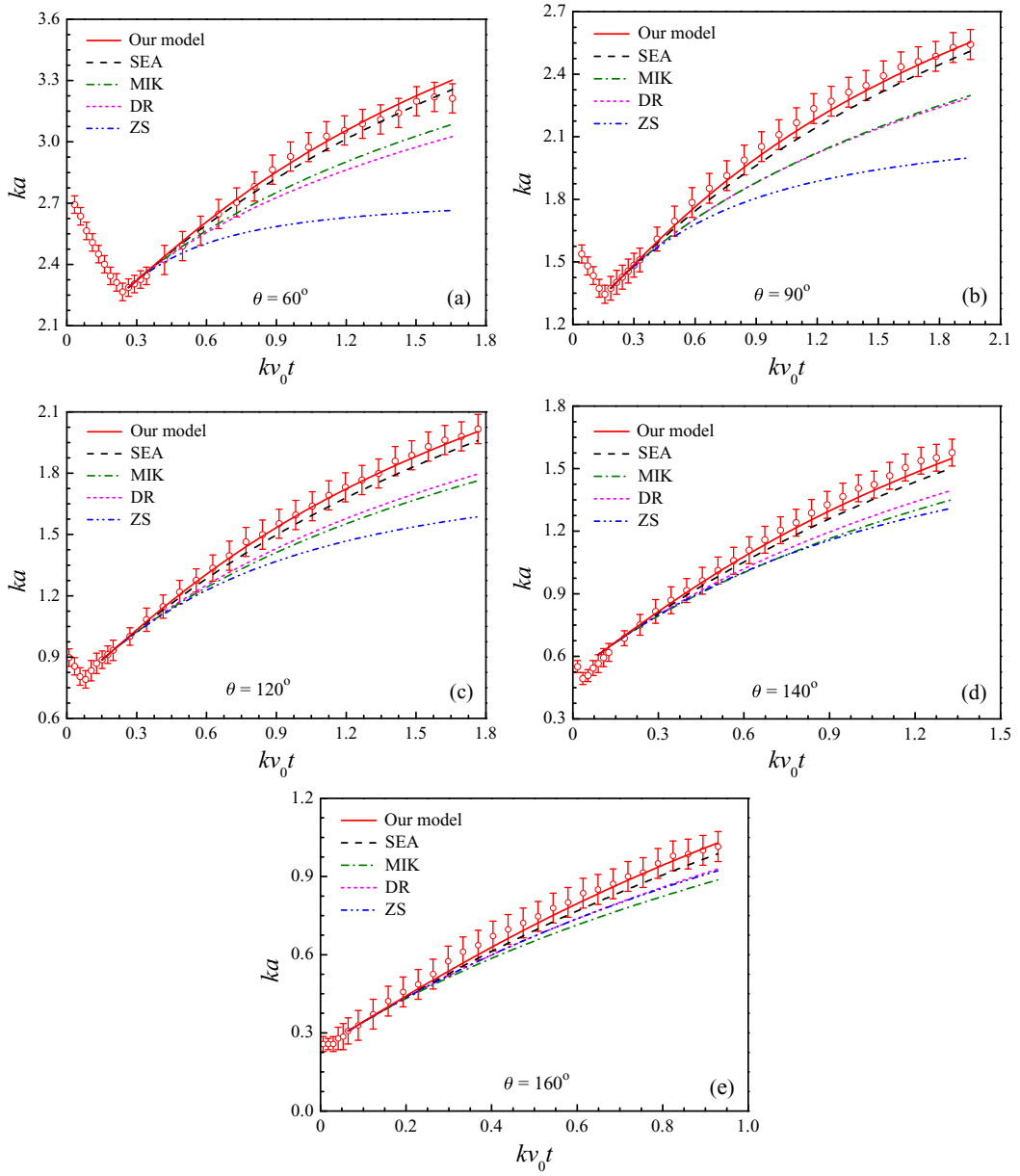

FIG. 7. Comparisons of width growth in linear and nonlinear stages between experiments and predictions from five models for $\theta = 60^\circ$, 90°, 120°, 140°, and 160°, respectively. Symbols represent the experimental results, and lines represent theoretical predictions.

is introduced to describe the observed reduction in spike acceleration for large ka_0^+, and the authors found that spikes are much more sensitive to ka_0^+ than bubbles. The coefficient of τ is much more complicated than that in the SEA model. The DR model can capture the asymptotic width growth in cases with a wide variety of $|A^+|$ and ka_0^+. In our previous work [27], the DR model can well predict the nonlinear width growth of a chevron interface, which shows that a chevron interface shares some similarities to a single-mode interface. However, the DR model underestimates the width growth of the inverse-chevron interface, as illustrated in Fig. 7.

Recently, Zhang and Guo [15] proposed a new model (the ZG model) to capture the nonlinear growth rates of bubbles and spikes, which can be expressed as

$$v_{b/s}^{\mathrm{ZG}} = v_0 \frac{1}{1+\hat{\alpha}\tau}, \tag{8}$$

where

$$\hat{\alpha} = \frac{3}{4}\frac{(1+A^+)(3+A^+)}{[3+A^+ +\sqrt{2}(1+A^+)^{1/2}]}\frac{[4(3+A^+)+\sqrt{2}(9+A^+)(1+A^+)^{1/2}}{[(3+A^+)^2+2\sqrt{2}(3-A^+)(1+A^+)^{1/2}]}$$

with the positive Atwood number for bubbles and its negative counterpart for spikes with the same density ratio. As presented in the work of Zhang and Guo [15], the ZG model provided a good prediction for the results of Sohn [39], Dimonte and Ramaprabhu [12], and Alon *et al.* [40]. However, the ZG model with $\hat{\alpha}$ a function of A^+ is similar to the MIK model in form, and it is not strange that the ZG model also fails to capture the nonlinear growth of the inverse-chevron interface in this work, as presented in Fig. 7.

In the work of Dimonte and Ramaprabhu [12], comparison of theoretical growth rates predicted by the SEA, DR, and MIK models with experimental counterparts [10,11,41] was made for single-mode interfaces. The results indicated that these models can all provide a good prediction of width growth at early stages, while only the DR model works well at late stages. Further comparison with the experiments [41] showed that the SEA model overestimates the bubble width growth, while the MIK model slightly underestimates it. Overall, for bubble width growth, the previous work indicated that the SEA model provides the largest growth rate while the DR and MIK models provide similar predictions in some cases. These results are consistent with our present findings, as indicated in Fig. 7. Zhang and Guo [15] showed that the ZG model gives a similar prediction to the DR model, which is correct for the inverse-chevron interface with small amplitudes, such as for $\theta = 140^\circ$ and 160°. For the inverse-chevron interface in this work, these models can predict the width growth to some extent, which illustrates that the inverse-chevron interface shares some similarities with single-mode interfaces. However, all models underestimate the asymptotic velocity of width growth, indicating that the width of an inverse-chevron interface grows much faster than that of a single-mode interface. As indicated in previous work [16,27,43], a chevron interface can be expressed in the form of a Fourier expansion. The fundamental mode, which has a wavelength equal to the opening of the chevron interface, contains ~81% of the mode, and the other infinitely many shorter modes make up the remaining 19%. Probably, the other shorter modes promote the width growth of the inverse-chevron interface. Moreover, the existence of a sharp corner and flat segments at both sides of the inverse-chevron interface may also influence the width growth. Those features were not considered in previous nonlinear models, and they require further investigations.

Note that all models mentioned above underestimate the asymptotic velocity of the width growth, and as $t \to \infty$ these models have a similar expression:

$$v_b \to \frac{1}{Ekt}, \tag{9}$$

where the value of E is different for each model, as listed in Table III. To better capture the asymptotic velocity of width growth of an inverse-chevron interface, we find that when E in Eq. (9) takes the form of $1 + (A^+/2)$, which is from the work of Sohn [42], the asymptotic velocity of width growth can be well-predicted. Based on the initial linear velocity and the asymptotic velocity, a model can be established as

$$v_b = v_0 \frac{1+E\tau}{1+E\tau+E^2\tau^2}. \tag{10}$$

As presented in Fig. 7, it is clear that the new model works well for predicting width growth in linear and weakly nonlinear phases. However, further investigations are needed to determine whether this model is applicable for other types of interfaces.

TABLE III. The values of E for different models.

Models	Specific form of E	Provenance of E
SEA	$[(1 \pm A^+)/(1 + A^+)][1/(2\pi C)]$	Alon *et al.* [40]
MIK	$3(1 + A^+)/(3 + A^+)$	Goncharov [38]
DR	$1 \pm \lvert A^+ \rvert$	Niederhaus *et al.* [41]
ZG	$\hat{\alpha}$	Zhang and Guo [15]
Our model	$(2 + A^+)/2$	Sohn [42]

IV. CONCLUSIONS

The width growth of an inverse-chevron air/SF_6 interface subjected to a weak shock wave is investigated experimentally in an attempt to figure out the difference in width growth between chevron and inverse-chevron interfaces. The inverse-chevron interface is created by the soap film technique, and the shocked interface morphology is captured by high-speed Schlieren photography.

For small vertex angles, more baroclinic vorticity is generated, and the interface deforms greatly with the formation of an obvious vortex pair. The vortex spacing changes continuously because the vortex pair swallows the small vortices on oblique interfaces. The width growths in linear and nonlinear phases are obtained. In the linear stage, the width growth in experiments with small initial amplitudes can be predicted by the impulsive model. For high initial amplitudes, a revised linear model considering a reduction factor can give a reasonable prediction. The linear growth rate is also a nonmonotone function of the initial vertex angle, which is consistent with our previous work [27]. However, the amplitude-wavelength ratio corresponding to the maximum linear growth rate is larger than the counterpart in our previous work due to the slight difference in Atwood number, which is consistent with the statement by Dell *et al.* [29]. At late stages, the weakly nonlinear behavior of width growth is observed, while in our previous work [27] the nonlinear behavior almost does not emerge, although the evolving duration is nearly the same. In this work, four typical nonlinear models are adopted to estimate the asymptotic velocity of width growth. All of them show a correct tendency of width growth, which indicates that an inverse-chevron interface shares some similarities with single-mode interfaces. However, all models underestimate the width growth rate, probably because they were derived based on single-mode interfaces and the roles of other high-order harmonic modes, which were initially presented in the inverse-chevron interface, are not considered. An empirical nonlinear model is proposed, which well reflects the asymptotic behaviors of width growth of an inverse-chevron interface. We note that its range of validity needs to be examined in future work.

The results in this work show that diversities exist between multimode interfaces with sharp corners and single-mode interfaces, and the coupling and competition of different modes play important roles in the interface evolution. In future work, the chevron interfaces with different wavelengths will be arranged alternatively to investigate the mode coupling and competition. The existence of flat segments at both sides of the inverse-chevron interface breaks the periodicity of the interface, and will likely affect the width growth, which will also be discussed in the near future.

ACKNOWLEDGMENTS

This work was partly supported by the National Natural Science Foundation of China (Grants No. 11772329, No. 11625211, and No. NSAF U1530103), the Science Challenge Project (No. TZ2016001), and the Fundamental Research Funds for the Central Universities under Grant No. WK2320000038.

[1] R. D. Richtmyer, Taylor instability in shock acceleration of compressible fluids, Commun. Pure Appl. Math. **13**, 297 (1960).
[2] E. E. Meshkov, Instability of the interface of two gases accelerated by a shock wave, Fluid Dyn. **4**, 101 (1969).
[3] J. Lindl, O. Landen, J. Edwards, E. Moses, and N. Team, Review of the national ignition campaign 2009-2012, Phys. Plasmas **21**, 020501 (2014).
[4] B. A. Remington, J. Kane, R. P. Drake, S. G. Glendinning, K. Estabrook, R. London, J. Castor, R. J. Wallace, D. Arnett, E. Liang, R. McCray, A. Rubenchik, and B. Fryxell, Supernova hydrodynamics experiments on the Nova laser, Phys. Plasmas **4**, 1994 (1997).
[5] N. J. Zabusky, Vortex paradigm for accelerated inhomogeneous flows: Visiometrics for the rayleigh-taylor and richtmyer-meshkov environments, Annu. Rev. Fluid Mech. **31**, 495 (1999).
[6] M. Brouillette, The Richtmyer-Meshkov instability, Annu. Rev. Fluid Mech. **34**, 445 (2002).
[7] D. Ranjan, J. Oakley, and R. Bonazza, Shock-bubble interactions, Annu. Rev. Fluid Mech. **43**, 117 (2011).
[8] X. Luo, Z. Zhai, T. Si, and J. Yang, Experimental study on the interfacial instability induced by shock waves, Adv. Mech. **44**, 260 (2014).
[9] Z. Zhai, L. Zou, Q. Wu, and X. Luo, Review of experimental Richtmyer-Meshkov instability in shock tube: From simple to complex, Proc. IMechE Pt. C: J. Mech. Eng. Sci. **232**, 2830 (2018).
[10] O. Sadot, L. Erez, U. Alon, D. Oron, L. A. Levin, G. Erez, G. Ben-Dor, and D. Shvarts, Study of Nonlinear Evolution of Single-Mode and Two-Bubble Interaction Under Richtmyer-Meshkov Instability, Phys. Rev. Lett. **80**, 1654 (1998).
[11] J. W. Jacobs and V. V. Krivets, Experiments on the late-time development of single-mode Richtmyer-Meshkov instability, Phys. Fluids **17**, 034105 (2005).
[12] G. Dimonte and P. Ramaprabhu, Simulations and model of the nonlinear Richtmyer-Meshkov instability, Phys. Fluids **22**, 014104 (2010).
[13] K. O. Mikaelian, Limitations and failures of the Layzer model for hydrodynamic instabilities, Phys. Rev. E **78**, 015303 (2008).
[14] M. Vandenboomgaerde, D. Souffland, C. Mariani, L. Biamino, G. Jourdan, and L. Houas, An experimental and numerical investigation of the dependency on the initial conditions of the Richtmyer-Meshkov instability, Phys. Fluids **26**, 024109 (2014).
[15] Q. Zhang and W. Guo, Universality of finger growth in two-dimensional Rayleigh-Taylor and Richtmyer-Meshkov instabilities with all density ratios, J. Fluid Mech. **786**, 47 (2016).
[16] K. O. Mikaelian, Richtmyer-Meshkov instability of arbitrary shapes, Phys. Fluids **17**, 034101 (2005).
[17] A. M. Abd-el Fattah and L. F. Henderson, Shock waves at a fast-slow gas interface, J. Fluid Mech. **86**, 15 (1978).
[18] A. M. Abd-el Fattah and L. F. Henderson, Shock waves at a slow-fast gas interface, J. Fluid Mech. **89**, 79 (1978).
[19] Z. G. Zhai, W. Li, T. Si, X. S. Luo, J. M. Yang, and X. Y. Lu, Refraction of cylindrical converging shock wave at an air/helium gaseous interface, Phys. Fluids **29**, 016102 (2017).
[20] A. Rikanati, D. Oron, O. Sadot, and D. Shvarts, High initial amplitude and high Mach number effects on the evolution of the single-mode Richtmyer-Meshkov instability, Phys. Rev. E **67**, 026307 (2003).
[21] J. A. McFarland, J. A. Greenough, and D. Ranjan, Computational parametric study of a Richtmyer-Meshkov instability for an inclined interface, Phys. Rev. E **84**, 026303 (2011).
[22] J. A. McFarland, J. A. Greenough, and D. Ranjan, Investigation of the initial perturbation amplitude for the inclined interface Richtmyer-Meshkov instability, Phys. Scr. **T155**, 014014 (2013).
[23] J. A. McFarland, D. Reilly, S. Creel, C. McDonald, T. Finn, and D. Ranjan, Experimental investigation of the inclined interface Richtmyer-Meshkov instability before and after reshock, Exp. Fluids **55**, 1640 (2014).
[24] J. A. McFarland, D. Reilly, W. Black, J. A. Greenough, and D. Ranjan, Modal interactions between a large-wavelength inclined interface and small-wavelength multimode perturbations in a Richtmyer-Meshkov instability, Phys. Rev. E **92**, 013023 (2015).
[25] R. Samtaney and N. J. Zabusky, Circulation deposition on shock-accelerated planar and curved density-stratified interfaces: models and scaling laws, J. Fluid Mech. **269**, 45 (1994).

[26] S. Zhang, G. Peng, and N. Zabusky, Vortex dynamics and baroclinically forced inhomogeneous turbulence for shock-planar heavy curtain interactions, J. Turbulence **6**, N3 (2005).
[27] X. Luo, P. Dong, T. Si, and Z. Zhai, The Richtmyer-Meshkov instability of a 'V' shaped air/SF_6 interface, J. Fluid Mech. **802**, 186 (2016).
[28] Z. Zhai, P. Dong, T. Si, and X. Luo, The Richtmyer-Meshkov instability of a 'V' shaped air/helium interface subjected to a weak shock, Phys. Fluids **28**, 082104 (2016).
[29] Z. Dell, R. F. Stellingwerf, and S. I. Abarzhi, Effect of initial perturbation amplitude on Richtmyer-Meshkov flows induced by strong shocks, Phys. Plasmas **22**, 092711 (2015).
[30] X. Luo, M. Wang, T. Si, and Z. Zhai, On the interaction of a planar shock with an SF_6 polygon, J. Fluid Mech. **773**, 366 (2015).
[31] M. Wang, T. Si, and X. Luo, Generation of polygonal gas interfaces by soap film for Richtmyer-Meshkov instability study, Exp. Fluids **54**, 1427 (2013).
[32] Z. Zhai, M. Wang, T. Si, and X. Luo, On the interaction of a planar shock with a light polygonal interface, J. Fluid Mech. **757**, 800 (2014).
[33] G. R. Baker, D. I. Meiron, and S. A. Orszag, Vortex simulations of the Rayleigh-Taylor instability, Phys. Fluids **23**, 1485 (1980).
[34] B. D. Collins and J. W. Jacobs, PLIF flow visualization and measurements of the Richtmyer-Meshkov instability of an air/SF_6 interface, J. Fluid Mech. **464**, 113 (2002).
[35] G. Jourdan and L. Houas, High-Amplitude Single-Mode Perturbation Evolution at the Richtmyer-Meshkov Instability, Phys. Rev. Lett. **95**, 204502 (2005).
[36] K. O. Mikaelian, Explicit expressions for the evolution of single-mode Rayleigh-Taylor and Richtmyer-Meshkov instabilities at arbitrary Atwood numbers, Phys. Rev. E **67**, 026319 (2003).
[37] D. Oron, L. Arazi, D. Kartoon, A. Rikanati, U. Alon *et al.*, Dimensionality dependence of the Rayleigh-Taylor and Richtmyer-Meshkov instability late-time scaling laws, Phys. Plasmas **8**, 2883 (2001).
[38] V. N. Goncharov, Analytical Model of Nonlinear, Single-Mode, Classical Rayleigh-Taylor Instability at Arbitrary Atwood Numbers, Phys. Rev. Lett. **88**, 134502 (2002).
[39] S. I. Sohn, Vortex model and simulations for Rayleigh-Taylor and Richtmyer-Meshkov instability, Phys. Rev. E **69**, 036703 (2004).
[40] U. Alon, J. Hecht, D. Ofer, and D. Shvarts, Power Laws and Similarity of Rayleigh-Taylor and Richtmyer-Meshkov Mixing Fronts, Phys. Rev. Lett. **74**, 534 (1995).
[41] C. E. Niederhaus and J. W. Jacobs, Experimental study of the Richtmyer-Meshkov instability of incompressible fluids, J. Fluid Mech. **485**, 243 (2003).
[42] S. I. Sohn, Simple potential-flow model of Rayleigh-Taylor and Richtmyer-Meshkov instabilities for all density ratios, Phys. Rev. E **67**, 026301 (2003).
[43] K. O. Mikaelian, Functions $\sin_k x$ and $\cos_k x$, J. Phys. A **26**, 1673 (1993).